Mechanical Systems and Signal Processing 168 (2022) 108739

Contents lists available at ScienceDirect

Mechanical Systems and Signal Processing

journal homepage: www.elsevier.com/locate/ymssp

A continuous contact force model for impact analysis

Jie Zhang [a,*], Xu Liang [a], Zhonghai Zhang [b], Guanhua Feng [c,d], Quanliang Zhao [a], Lei Zhao [a], Guangping He [a,*]

[a] School of Mechanical and Materials Engineering, North China University of Technology, No.9, Jinyuanzhuang Road, Shijingshan District, Beijing 100144, China
[b] Beijing Aerospace Measurement & Control Technology Co., Ltd., No.3 Shixingdong Road, Shijingshan District, Beijing 100041, China
[c] Institute of Mechanics, Chinese Academy of Sciences, No.15 Beisihuanxi Road, Haidian District, Beijing 100190, China
[d] School of Engineering Science, University of Chinese Academy of Sciences, No.19(A) Yuquan Road, Shijingshan District, Beijing 100049, China

ARTICLE INFO

Keywords:
Contact model
Impact
Approximate dynamic equation

ABSTRACT

Hunt and Crossley proposed a general expression of the contact force in 1975. The dissipative force term of the general expression has two exponents: the exponent of indentation depth and that of velocity. Because it is almost impossible to obtain an analytical solution based on the general expression, more than twenty continuous contact models have been developed based on the simplification of the general expression. In these studies, the exponent of the indentation depth was set as 0.25, 0.5, 0.65, 1.0 or 1.5, and the exponent of the velocity was set to 1.0. This paper proposes a new continuous contact force model with arbitrary values of the exponents of the indentation depth and velocity. The model is based on the general expression of the contact force. Considering the rule of energy equivalence, an approximate dynamic equation is developed by introducing the equivalent indentation and equivalent velocity. Subsequently, a new continuous contact force model is constructed based on the system dynamic equation and approximate dynamic equation. The influences of the two exponents on the performance of the continuous contact force models are investigated by analyzing the simulation results. Moreover, the validity of the new model is demonstrated by comparing the simulation results with two published experimental datasets. The comparison also indicates that the performance of the continuous contact model can be enhanced by selecting appropriate values of the two exponents.

1. Introduction

In recent years, extensive research has been performed to examine the modeling of contact-impact phenomena [1–5], which are commonly found in nature and frequently occur in mechanical systems [6–9]. The compliant continuous contact force method is a powerful tool to simulate contact-impact problems [10,11]. More than twenty continuous contact models have been presented thus far [2,10–12]. Applications of such models include simulations of robots [10], vehicles, droplets [13], robotic arms [14], sand particles [15], clay, seeds [16], hail specimens [17], structural pounding during earthquakes, aeroengines [18] and contact processes between the barrel and bourrelet of projectiles [19]. Moreover, such models have been applied in simulations of the discrete element method and smoothed particle hydrodynamics [11].

Fig. 1 shows the development of the continuous contact force model. In 1880, Hertz proposed the Hertz contact model [20], which

* Corresponding authors.
E-mail addresses: zhangjie@ncut.edu.cn (J. Zhang), hegp55@126.com (G. He).

https://doi.org/10.1016/j.ymssp.2021.108739
Received 27 August 2021; Received in revised form 4 December 2021; Accepted 7 December 2021
Available online 20 December 2021

Nomenclature

F_c	normal contact force
δ, δ_{max}	deformation or indentation, maximum indentation
$\dot{\delta}$, $\ddot{\delta}$	deformation velocity or indentation velocity, indentation acceleration
k, λ	contact stiffness, hysteresis damping factor
n	elastic term exponent
m	damping term exponent of indentation depth
q	damping term exponent of indentation velocity
$\dot{\delta}^{(-)}$, $\dot{\delta}^{(+)}$	initial indentation velocity, relative separation velocity
$t^{(-)}$, $t^{(+)}$, tm	time of initial contact, time of separation, time of maximum indentation
m_0	mass
$\widehat{\delta}$	equivalent indentation depth
$\dot{\widehat{\delta}}$, $\dot{\widehat{\delta}}_c$, $\dot{\widehat{\delta}}_r$	equivalent velocity, equivalent velocity of compression phase, equivalent velocity of restitution phase
c_r	coefficient of restitution
ΔE_c, ΔE_r	energy loss for compression or restitution phase calculating based on the system dynamic equation
ΔE_c^*, ΔE_r^*	energy loss for compression or restitution phase calculating based on the approximate dynamic equation
ΔE_{loss}	energy loss
ΔE_k	elastic potential energy
x, τ	non-dimensional variables
$\dot{x}$, $\ddot{x}$	derivative of x with respect to τ, derivative of $\dot{x}$ with respect to τ
k_{non}, λ_{non}	non-dimensional parameters of the system dynamic equation
k_{non}^*, λ_{non}^*	non-dimensional parameters of the approximate dynamic equation

defined the contact force F_c as a function of the indentation depth δ: $F_c = k\delta^n$, where k represents the stiffness parameter, and the exponent n depends on the topological properties of the contacting surfaces [21]. Hertz derived the analytical expression for k and the values of n when two spheres are in static contact; this model has been widely used in many fields [13,22]. In addition, the Hertz model can be used to describe quasistatic contact problems of geometrical bodies other than spheres, and the corresponding n values and k expressions have been clarified [23]. However, the Hertz model does not consider energy dissipation, which almost inevitably occurs during a collision [21].

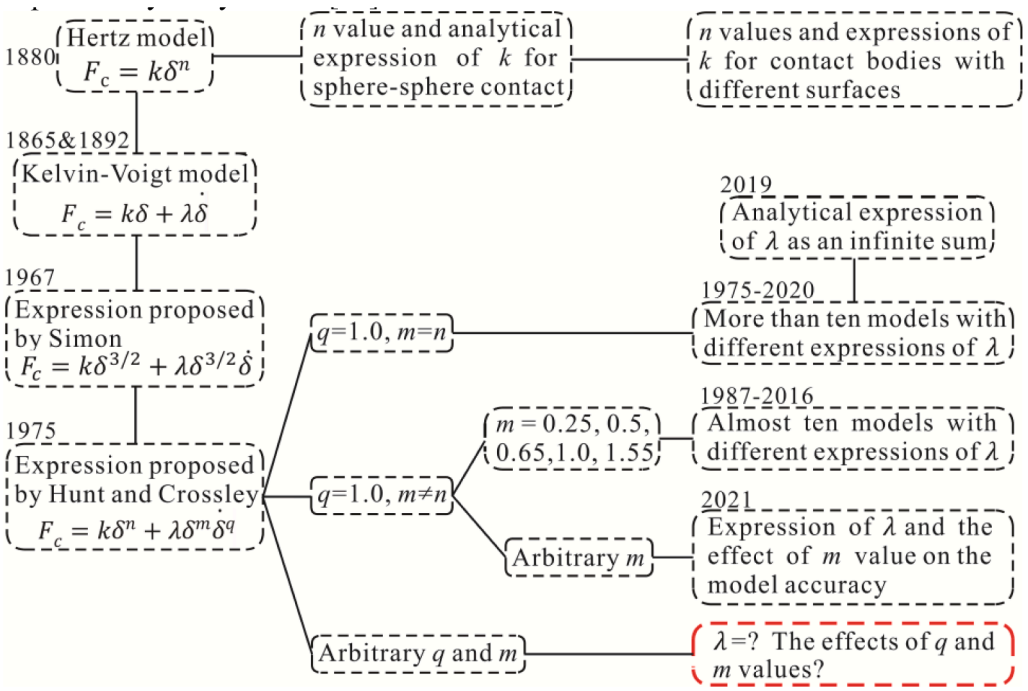

Fig. 1. The development of the continuous contact force model.

By introducing a damping term $\lambda\dot{\delta}$ (where $\dot{\delta}$ is the velocity of the indentation depth and λ is the hysteresis damping factor), the Kelvin–Voigt model can simulate the energy dissipation in contact-impact processes [24,25]. However, at the initial and separation moments of the collision, the contact force calculated using the Kelvin–Voigt model is nonzero when the deformation is zero, which is not consistent with the actual behavior [26]. Another drawback of this model is that it produces the wrong sign for the contact force at the end of the impact [27]. Moreover, the accuracy of this model is relatively low.

In 1967, Simon proposed a nonlinear contact force model when studying the performance of golf clubs. In this model, the exponent $n = 1.5$, and the expression of contact force is $F_c = k\delta^{3/2} + \lambda\delta^{3/2}\dot{\delta}$ [27,28].

In 1975, Hunt and Crossley proposed a general expression of the contact force, which is expressed as $F_c = k\delta^n + \lambda\delta^m\dot{\delta}^q$ [29]. In the case of static contact, $\dot{\delta}$ equals zero, and the equation is simplified to the Hertz model. In the case of impact processing, the damping term $\lambda\delta^m\dot{\delta}^q$ is used to describe the energy dissipation, and the contact force in this equation is consistent with the actual behavior. The research of Hunt and Crossley has inspired a large number of researchers and led to numerous methods to evaluate contact forces [1,2,10–12,30,31], and the crucial step in the construction of these models is the determination of the expression of λ. Notably, because it is almost impossible to find an analytical solution to λ based on the general expression, assumptions about the exponential values have been introduced to simplify the general equation, and contact force models have been developed based on the corresponding simplified equations.

Based on the assumptions of $m = n$ and $q = 1.0$, Hunt and Crossley simplified the general equation as $F_c = k\delta^n + \lambda\delta^n\dot{\delta}$. The simplified equation is usually called the Hunt-Crossley model; in some research, it is also called the Simon-Hunt-Crossley model. In recent years, more than ten continuous contact models have been developed on the basis of this simplified equation [21,26,29,32–45], such as the influential models proposed by Lankarani and Nikravesh [36]. However, Hunt and Crossley still pointed out that "the index q need not be taken as unity" [29]. In 2019, based on the simplified expression $F_c = k\delta^n + \lambda\delta^n\dot{\delta}$, an analytic solution of λ in the form of an infinite series was presented [46].

On the other hand, approximately ten models have been developed based on the other simplified equation $F_c = k\delta^n + \lambda\delta^m\dot{\delta}$, in which $m \neq n$ and $q = 1.0$. In these studies, the value of m was set as 0.25 [47], 0.5 [48–51], 0.65 [41], 1.0 [52–54], and 1.55 [55], with n equal to 1.5. Among them, Kuwabara-Kono's model is a typical model derived from elasticity theory, and the value of m equals 0.5 [48]; however, it has been pointed out that this model produces contact forces with erroneous signs before the end of the impact [27]. In 2021, Jie Zhang et al. developed a new continuous contact force model [31]. In this study, $q = 1.0$, and the value of m was arbitrary. Moreover, the authors investigated the effect of m on the accuracy of the contact force model.

Several studies also considered the case in which q is not 1.0. Ebrahim Alizadeh et al. developed a granular normal contact force model for a dashpot filled with a non-Newtonian liquid; in this study, $n = 1.5$ and $m = 1.0$, q was a variable, and the values of hysteresis damping factor λ and q were determined by fitting experimental data [56]. Liang Ding et al. studied the foot–terrain interaction mechanics for legged robots based on the general expression of the contact force. However, the values of λ, m and q were identified according to the experimental results, and no formula for calculating λ was specified [57].

According to the development progress of the continuous contact force model, as shown in Fig. 1, most of the existing studies have been based on the simplified general expression of the contact force, and the parameter q was set as 1.0 because the general expression $F_c = k\delta^n + \lambda\delta^m\dot{\delta}^q$ cannot be used to find an analytical solution [1,2,29]. In this regard, it is of significance to develop a contact model based on the general expression of the contact force with arbitrary values of parameters n, m and q. This study considers this aspect and proposes a new type of continuous contact force model with arbitrary exponents n, m and q. Moreover, the effects of the values of m and q on the performance of the continuous contact force models are discussed.

The remaining paper is organized as illustrated in Fig. 2. The development of the new model is described in Section 2, as shown in the blue box in Fig. 2. Section 2.1 covers the fundamentals of the continuous contact force models. Next, in Section 2.2, an approximate equation is established based on the rule of energy equivalence. Then, the expression of the hysteresis damping factor λ is derived in Section 2.3, which is crucial for the construction of the new model. The data analysis and validation of the new model are described in Section 3, as shown in the red box in Fig. 2. First, a nondimensional analysis is performed in Section 3.1. Then, numerical simulations

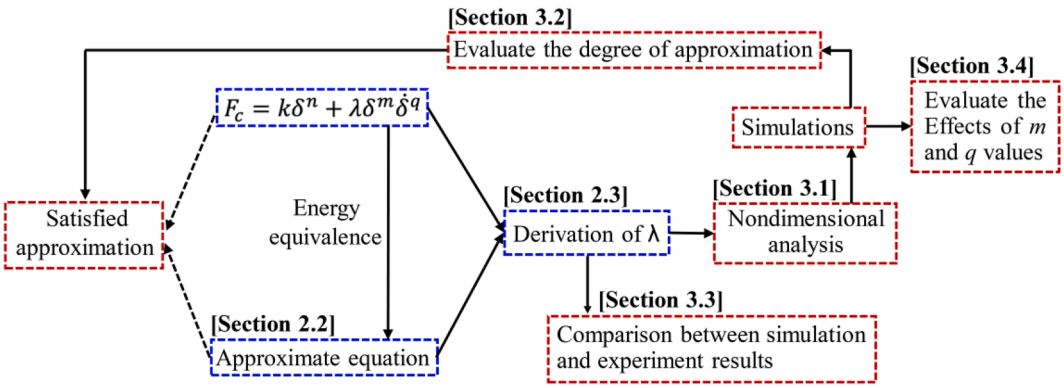

Fig. 2. Structure of this research.

are conducted with different values of exponents n, m, and q and restitution coefficient c_r, and the evaluation of the degree of approximation reveals the feasibility of the approximate equation, as described in Section 3.2. In Section 3.3, the model is validated by comparing the simulation data with two published experimental datasets. Finally, the effects of m and q on the performance of the contact models are investigated in Section 3.4.

2. Development of the new model

2.1. General issues regarding the construction of the new model

Fig. 3 shows the schematic diagram of the impact process and the corresponding modeling methods. As shown in Fig. 3(a), an impact between a solid object (with mass m_0) and half space is divided into two phases: the compression phase and the restitution phase. At the initial time of impact $t^{(-)}$, the object has initial velocity $\dot{\delta}^{(-)}$; the deformation takes place in the local contact zone and increases until the indentation depth reaches the maximum δ_{max} at time t_m, and the object velocity becomes zero. Then, the deformation begins to recover; at separation time $t^{(+)}$, the contact force becomes zero, and the velocity becomes $\dot{\delta}^{(+)}$. The period from $t^{(-)}$ to t_m is defined as the compression phase, and the period from t_m to $t^{(+)}$ is defined as the restitution phase, as shown in Fig. 3(a). The impact system demonstrated in Fig. 3(a) can be treated as equivalent to the systems of most elastic contact-impact problems [21,23], as the contact area is much smaller than the sizes of the contacting objects.

Fig. 3(b–d) show schematics of the continuous contact force models. Fig. 3(b) shows the Hertz model, which is a purely elastic model and cannot simulate the energy dissipation [20]. Fig. 3(c) shows a schematic of the continuous contact model with damping that can simulate the energy dissipation. The general expression of this type of contact model is $F_c = k\delta^n + \lambda\delta^m\dot{\delta}^q$; $k\delta^n$ is the elastic force term, and $\lambda\delta^m\dot{\delta}^q$ is the dissipative force term. As $m = 0$, $n = 1.0$ and $q = 1.0$, the general expression degenerates to the Kelvin–Voigt model [24,25]. As $m = n$ and $q = 1.0$, an analytic solution of λ can be presented in the form of an infinite series [46]. It is almost impossible to obtain an analytical solution based on the general expression $m \neq n$. Jie Zhang et al. derived the expression for λ considering arbitrary values for m and $q = 1.0$ (in this case, the general expression degenerates to $F_c = k\delta^n + \lambda\delta^m\dot{\delta}$) based on an approximate contact force equation established based on the rule of energy equivalence [31]. As shown in Fig. 3(d), the approximate contact force equation adopts the form of a "rigid spring in compression phase + soft spring in restitution phase" to simulate the energy dissipation, thereby eliminating the nonlinear dissipative force term $\lambda\delta^m\dot{\delta}^q$ in the continuous model. The comparison between the simulation results and published experimental data showed that this new model achieves high accuracy (<5%) [31]. Inspired by the work of Jie Zhang et al. [31], this paper proposes a new type of continuous contact force model developed based on the general contact force equation $F_c = k\delta^n + \lambda\delta^m\dot{\delta}^q$ (in this case, m does not have to equal n, and q does not have to equal 1.0). Moreover, the effects of the values of m and q on the performance and accuracy of the continuous contact force models are investigated.

According to the general contact force equation $F_c = k\delta^n + \lambda\delta^m\dot{\delta}^q$, the dynamic equation for the contact-impact system, as illustrated in Fig. 3(a), can be obtained:

$$m_0\ddot{\delta} + k\delta^n + \lambda\delta^m\dot{\delta}^q = 0 \tag{1}$$

where the gravity term is ignored because it is considerably smaller than the impact force. m_0 is the mass or equivalent mass of the

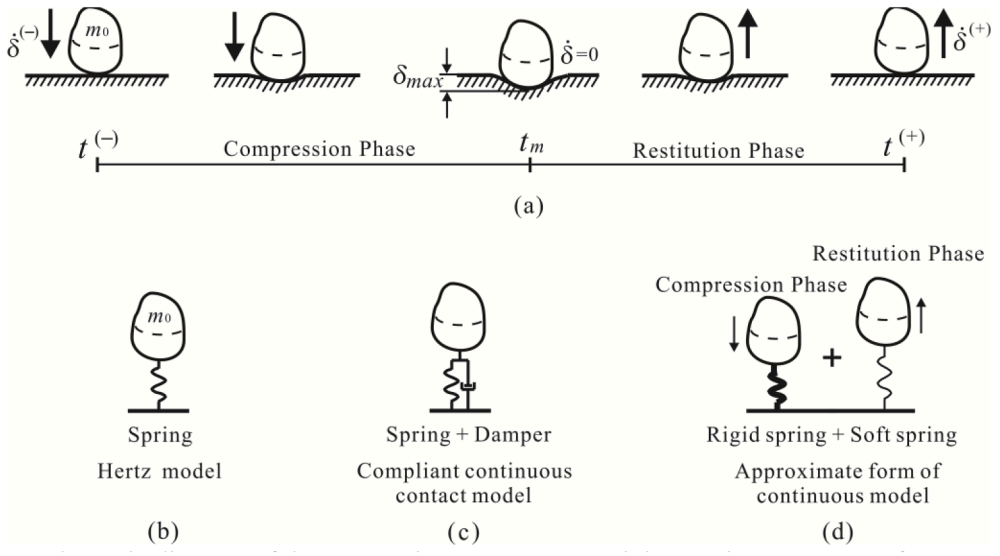

Fig. 3. Schematic diagram of the contact-impact process and the continuous contact force models.

contact bodies [31], k represents the generalized stiffness parameter, and exponent n depends on the topological properties of the contacting surfaces [15]. Details regarding the determination of the values of m_0, k and n for different contact-impact problems can be found in the relevant articles [23,31].

2.2. Development of the approximate dynamic equation

In this section, an approximate dynamic equation for the impact system is developed according to the rule of energy equivalence. Subsequent analysis in Sections 2.2 and 3.2 reveals that it achieves a good approximation of the system dynamic equation and is an important basis for the construction of a new contact model.

To develop the approximate dynamic equation, the system dynamic equation expressed by Eq. (1) can be rewritten as

$$m_0\ddot{\delta}+\left(\delta^{n-m}+\frac{\lambda}{k}\dot{\delta}^{q}\right)k\delta^{m}=0 \tag{2}$$

By introducing equivalent indentation and equivalent velocity, a primary formula of the approximate dynamic equation can be constructed:

$$m_0\ddot{\delta}+\left(\widehat{\delta}^{n-m}+\frac{\lambda}{k}\widehat{\dot{\delta}}^{q}\right)k\delta^{m}=0 \tag{3}$$

where $\widehat{\delta}$ is the equivalent indentation depth, which is associated with the maximum indentation depth δ_{max}. $\widehat{\dot{\delta}}$ is the equivalent velocity. More details will be discussed in the following sections.

As illustrated in Fig. 3(d), the energy dissipation can be simulated by setting different stiffness coefficients in the compression and restitution phases. The approximate dynamic equation is constructed based on the form of a "rigid spring in the compression phase + soft spring in the restitution phase", as shown in Eq. (4).

$$\begin{cases} m_0\ddot{\delta}+\left(\widehat{\delta}^{n-m}+\frac{\lambda}{k}(\widehat{\dot{\delta}}_c)^{q}\right)k\delta^{m}=0\text{Compressionphase} \\ m_0\ddot{\delta}+\left(\widehat{\delta}^{n-m}+\frac{\lambda}{k}(\widehat{\dot{\delta}}_r)^{q}\right)k\delta^{m}=0\text{Restitutionphase} \end{cases} \tag{4}$$

where $\widehat{\dot{\delta}}_c$ and $\widehat{\dot{\delta}}_r$ are the equivalent velocities of the compression and restitution phases, respectively, which remain constant during the compression and restitution phases and are associated with $\dot{\delta}^{(-)}$.

The approximate dynamic equation of the compression phase can be expressed as

$$m_0\frac{d\dot{\delta}}{dt}+\left(\widehat{\delta}^{n-m}+\frac{\lambda}{k}(\widehat{\dot{\delta}}_c)^{q}\right)k\delta^{m}=m_0\frac{d\dot{\delta}}{d\delta}\frac{d\delta}{dt}+\left(\widehat{\delta}^{n-m}+\frac{\lambda}{k}(\widehat{\dot{\delta}}_c)^{q}\right)k\delta^{m}=0 \tag{5}$$

Which can then be rewritten as

$$m_0\dot{\delta}d\dot{\delta}=-\left(\widehat{\delta}^{n-m}+\frac{\lambda}{k}(\widehat{\dot{\delta}}_c)^{q}\right)k\delta^{m}d\delta=0 \tag{6}$$

By integrating Eq. (6) over the compression phase, it can be obtained that

$$\dot{\delta}^{2}-\dot{\delta}^{(-)^2}=-\frac{2k\left(\widehat{\delta}^{n-m}+\frac{\lambda}{k}(\widehat{\dot{\delta}}_c)^{q}\right)}{m_0(m+1)}\delta^{m+1} \tag{7}$$

As the indentation depth δ reaches the maximum value δ_{max} and the deformation velocity $\dot{\delta}=0$, it can be deduced that

$$\delta_{max}^{m+1}=-\frac{m_0(m+1)}{2k\left(\widehat{\delta}^{n-m}+\frac{\lambda}{k}(\widehat{\dot{\delta}}_c)^{q}\right)}\dot{\delta}^{(-)^2} \tag{8}$$

According to Eqs. (7) and (8), the function between deformation velocity $\dot{\delta}$ and indentation depth δ during the compression phase can be obtained

$$\dot{\delta}=\dot{\delta}^{(-)}\sqrt{1-\left(\frac{\delta}{\delta_{max}}\right)^{m+1}} \tag{9}$$

Based on Eq. (9), the work done by the dissipative force term $\lambda\delta^{m}\dot{\delta}^{q}$ during the compression phase can be calculated:

$$\Delta E_c = \int_0^{\delta_{max}} \lambda\delta^m \dot{\delta}^q d\delta = \int_0^{\delta_{max}} \lambda\delta^m \left(\dot{\delta}^{(-)} \sqrt{1-\left(\frac{\delta}{\delta_{max}}\right)^{m+1}} \right)^q d\delta = \int_0^1 \frac{\lambda\delta_{max}^{m+1}\left(\dot{\delta}^{(-)}\right)^q}{m+1} \left(\sqrt{1-\left(\frac{\delta}{\delta_{max}}\right)^{m+1}} \right)^q d\left(\frac{\delta}{\delta_{max}}\right)^{m+1}$$
$$= \int_0^1 \frac{\lambda\delta_{max}^{m+1}\left(\dot{\delta}^{(-)}\right)^q}{m+1} \left(\sqrt{1-x}\right)^q dx = \frac{\lambda\delta_{max}^{m+1}}{m+1} \cdot \frac{2\left(\dot{\delta}^{(-)}\right)^q}{2+q} \tag{10}$$

In addition, as described in Eq. (4), based on the approximate dynamic equation of the compression phase, the work done by the dissipative force term during the compression phase is obtained

$$\Delta E_c^* = \int_0^{\delta_{max}} \lambda\delta^m (\hat{\dot{\delta}}_c)^q d\delta = \frac{\lambda\delta_{max}^{m+1}}{m+1} (\hat{\dot{\delta}}_c)^q \tag{11}$$

Next, according to the rule of energy dissipation equivalence, the equivalent velocity during the compression phase can be determined based on Eqs. (10) and (11):

$$\hat{\dot{\delta}}_c = \left(\frac{2}{2+q}\right)^{\frac{1}{q}} \dot{\delta}^{(-)} \tag{12}$$

According to the system dynamic equation, the work done by the elastic force term $k\delta^n$ during the compression phase can be deduced:

$$\int_0^{\delta_{max}} k\delta^n d\delta = \frac{k\delta_{max}^{n+1}}{n+1} \tag{13}$$

According to the approximate dynamic equation of the compression phase, the work done by the elastic force term during the compression phase can be calculated based on Eq. (4):

$$\int_0^{\delta_{max}} k\delta^m \hat{\delta}^{n-m} d\delta = \frac{k\delta_{max}^{m+1}\hat{\delta}^{n-m}}{m+1} \tag{14}$$

Then, based on the rule of energy equivalence, the equivalent indentation depth can be determined according to Eqs. (13) and (14):

$$\hat{\delta}^{n-m} = \frac{m+1}{n+1}\delta_{max}^{n-m} \tag{15}$$

Similar to the analysis for the compression phase, the integration of Eq. (7) over the restitution phase yields

$$\left(c_r\dot{\delta}^{(-)}\right)^2 - \dot{\delta}^2 = \frac{2k\left(\hat{\delta}^{n-m} + \frac{\lambda}{k}(\hat{\dot{\delta}}_r)^q\right)}{m_0(m+1)}\delta^{m+1} \tag{16}$$

where c_r is the restitution coefficient. If $\dot{\delta} = 0$, the indentation depth δ reaches the maximum value δ_{max}, and it can be derived that

$$\delta_{max}^{m+1} = -\frac{m_0(m+1)}{2k\left(\hat{\delta}^{n-m} + \frac{\lambda}{k}(\hat{\dot{\delta}}_c)^q\right)}\left(c_r\dot{\delta}^{(-)}\right)^2 \tag{17}$$

The velocities of the restitution and compression phases have opposite directions, and thus, the function between the deformation velocity $\dot{\delta}$ and indentation depth δ during the restitution phase can be described as

$$\dot{\delta} = -c_r\dot{\delta}^{(-)}\sqrt{1-\left(\frac{\delta}{\delta_{max}}\right)^{m+1}} \tag{18}$$

The work done by the dissipative force term $\lambda\delta^m\dot{\delta}^q$ during the restitution phase is

$$\Delta E_r = \int_0^{\delta_{max}} \lambda\delta^m \dot{\delta}^q d\delta = -\int_{\delta_{max}}^0 \lambda\delta^m \left(c_r\dot{\delta}^{(-)} \sqrt{1-\left(\frac{\delta}{\delta_{max}}\right)^{m+1}} \right)^q d\delta = \frac{\lambda\delta_{max}^{m+1}}{m+1} \cdot \frac{2\left(c_r\dot{\delta}^{(-)}\right)^q}{2+q} \tag{19}$$

As described in Eq. (4), based on the approximate dynamic equation of the restitution phase, the work done by the dissipative force term during the restitution phase is

$$\Delta E_r^* = \int_{\delta_{max}}^0 \lambda\delta^m (\hat{\dot{\delta}}_r)^q d\delta = -\frac{\lambda\delta_{max}^{m+1}}{m+1}(\hat{\dot{\delta}}_r)^q \tag{20}$$

According to the rule of energy dissipation equivalence, the equivalent velocity during the restitution phase can be obtained based on Eqs. (19) and (20),

$$\hat{\dot{\delta}}_r = \left(\frac{-2}{2+q}\right)^{\frac{1}{q}} c_r \dot{\delta}^{(-)} \tag{21}$$

According to the system dynamic equation, the work done by the elastic force term $k\delta^n$ during the restitution phase can be deduced:

$$\int_{\delta_{max}}^{0} k\delta^n d\delta = -\frac{k\delta_{max}^{n+1}}{n+1} \tag{22}$$

Furthermore, based on the approximate dynamic equation of the restitution phase, the work done by the elastic force term during the restitution phase can be calculated based on Eq. (4),

$$\int_{\delta_{max}}^{0} k\delta^m \hat{\delta}^{n-m} d\delta = -\frac{k\delta_{max}^{m+1}\hat{\delta}^{n-m}}{m+1} \tag{23}$$

According to the rule of energy equivalence, the equivalent indentation depth can be obtained based on Eqs. (22) and (23), which is the same as Eq. (15),

$$\hat{\delta}^{n-m} = \frac{m+1}{n+1}\delta_{max}^{n-m} \tag{24}$$

Based on the above derivation, the expression for the approximate dynamic equation can be obtained by substituting Eqs. (12), (15), (21) and (24) into Eq. (4):

$$\begin{cases} m_0\ddot{\delta} + \left(\frac{m+1}{n+1}\delta_{max}^{n-m} + \frac{\lambda}{k}\left(\frac{2}{2+q}\right)\left(\dot{\delta}^{(-)}\right)^q\right)k\delta^m = 0 \text{ Compression phase} \\ m_0\ddot{\delta} + \left(\frac{m+1}{n+1}\delta_{max}^{n-m} - \frac{\lambda}{k}\left(\frac{2}{2+q}\right)\left(c_r\dot{\delta}^{(-)}\right)^q\right)k\delta^m = 0 \text{ Restitution phase} \end{cases} \tag{25}$$

Therefore, the approximate dynamic equation for the impact system can be determined based on the rule of energy equivalence.

2.3. Expression of the hysteresis damping factor

The determination of the expression of the hysteresis damping factor λ is a key step for the construction of the contact model. In this section, an analytical solution for λ is obtained based on the system dynamic equation and the approximate dynamic equation.

According to the law of conservation of linear momentum and energy balance, the total energy loss ΔE_{loss} can be described as in [58],

$$\Delta E_{loss} = \frac{1}{2}m_0\left(1-{c_r}^2\right)\dot{\delta}^{(-)^2} \tag{26}$$

As described in Section 2.2, Eqs. (10) and (19) are deduced from the system dynamic equation and the function $\dot{\delta}(\delta)$ which is derived from the approximate dynamic equation. On the basis of both equations, it can be deduced that

$$\frac{\Delta E_c}{\Delta E_r} = {c_r}^{-q} \tag{27}$$

Considering the total energy loss $\Delta E_{loss} = \Delta E_c + \Delta E_r$, substituting Eq. (27) into Eq. (26) yields

$$\Delta E_c = \frac{m_0\dot{\delta}^{(-)^2}(1-{c_r}^2)}{2(1+{c_r}^q)} \tag{28}$$

The elastic potential energy ΔE_k (the work done by the elastic force term) stored during the compression phase is

$$\Delta E_k = \int_0^{\delta_{max}} k\delta^n d\delta = \frac{k\delta_{max}^{n+1}}{n+1} \tag{29}$$

According to the energy balance of the compression phase, it can be deduced that

$$\frac{m_0\dot{\delta}^{(-)^2}}{2} = \Delta E_k + \Delta E_c = \frac{k\delta_{max}^{n+1}}{n+1} + \frac{m_0\dot{\delta}^{(-)^2}(1-{c_r}^2)}{2(1+{c_r}^q)} \tag{30}$$

which yields

$$\delta_{max}^{n+1} = \frac{m_0(n+1)\dot{\delta}^{(-)^2}}{2k}\bullet\frac{{c_r}^2+{c_r}^q}{1+{c_r}^q} \tag{31}$$

Substituting Eq. (31) into Eqs. (10) and (19), we obtain

$$\Delta E_c = \frac{\lambda}{m+1}\bullet\frac{2\left(\dot{\delta}^{(-)}\right)^{\mathrm{q}}}{2+\mathrm{q}}\left(\frac{\mathrm{m}_0(\mathrm{n}+1)\dot{\delta}^{(-)^2}}{2\mathrm{k}}\bullet\frac{\mathrm{c_r}^2+\mathrm{c_r}^{\mathrm{q}}}{1+\mathrm{c_r}^{\mathrm{q}}}\right)^{\frac{\mathrm{m}+1}{\mathrm{n}+1}} \tag{32}$$

and

$$\Delta E_r = \frac{\lambda}{m+1}\bullet\frac{2\left(\mathrm{c_r}\dot{\delta}^{(-)}\right)^{\mathrm{q}}}{2+\mathrm{q}}\left(\frac{\mathrm{m}_0(\mathrm{n}+1)\dot{\delta}^{(-)^2}}{2\mathrm{k}}\bullet\frac{\mathrm{c_r}^2+\mathrm{c_r}^{\mathrm{q}}}{1+\mathrm{c_r}^{\mathrm{q}}}\right)^{\frac{\mathrm{m}+1}{\mathrm{n}+1}} \tag{33}$$

Considering the total energy loss $\Delta E_{loss} = \Delta E_c + \Delta E_r$, according to Eqs. (26), (32) and (33), it can be deduced that

$$\left(\frac{m_0(n+1)\dot{\delta}^{(-)^2}}{2k}\bullet\frac{c_r{}^2+c_r{}^q}{1+c_r{}^q}\right)^{\frac{m+1}{n+1}}\left(\frac{2\lambda\left(\dot{\delta}^{(-)}\right)^q}{(m+1)(2+q)}+\frac{2\lambda\left(c_r\dot{\delta}^{(-)}\right)^q}{(m+1)(2+q)}\right)=\frac{m_0(1-c_r{}^2)\dot{\delta}^{(-)^2}}{2} \tag{34}$$

Then, the expression of the hysteresis damping factor λ can be obtained:

$$\lambda=\frac{m_0(2+q)(1-c_r{}^2)(m+1)\dot{\delta}^{(-)^2}}{4(\dot{\delta}^{(-)})^q(1+c_r{}^q)}\left(\frac{m_0(n+1)\dot{\delta}^{(-)^2}}{2k}\bullet\frac{c_r{}^2+c_r{}^q}{1+c_r{}^q}\right)^{-\frac{m+1}{n+1}} \tag{35}$$

In this manner, a new type of continuous contact force model can be proposed based on the general expression of the contact force, in which the values of exponents m and q can be arbitrary. When $q = 1.0$, the simplified expression of Eq. (35) is the same as Eq. (36) in article [31]. When $q = 1.0$ and $m = n$, the simplified expression of Eq. (35) is the same as Eq. (42) in article [21]. Based on Eqs. (1) and (35), a numerical simulation can be conducted, and the dynamic response of the impact process can be obtained. As mentioned above, details regarding the determination of the expression of stiffness parameter k can be found in the relevant articles [23,31]. It should be noted that the model proposed in this paper is only applicable to single-point impact and cannot be applied to multiple impacts. Like most continuous contact models, the new model includes an initial relative velocity term $\dot{\delta}^{(-)}$ in the expression of the damping factor, and the initial relative velocity between the contacting bodies is zero in most of multiple impacts, so the simulation of multiple impacts based on the new model will lead to infinite damping factor and thus obvious errors.

Additionally, by substituting Eq. (31) into Eq. (25), an exact expression of the approximate dynamic equation can be obtained:

$$\begin{cases} m_0\ddot{\delta}+\left(\frac{m+1}{n+1}\left(\frac{m_0(n+1)\dot{\delta}^{(-)^2}}{2k}\bullet\frac{c_r{}^2+c_r{}^q}{1+c_r{}^q}\right)^{\frac{m+1}{n+1}}+\frac{\lambda}{k}\left(\frac{2}{2+q}\right)\left(\dot{\delta}^{(-)}\right)^q\right)k\delta^m=0 \text{ Compression phase} m_0\ddot{\delta} \\ +\left(\frac{m+1}{n+1}\left(\frac{m_0(n+1)\dot{\delta}^{(-)^2}}{2k}\bullet\frac{c_r{}^2+c_r{}^q}{1+c_r{}^q}\right)^{\frac{m+1}{n+1}}-\frac{\lambda}{k}\left(\frac{2}{2+q}\right)\left(c_r\dot{\delta}^{(-)}\right)^q\right)k\delta^m=0 \text{ Restitution phase} \end{cases} \tag{36}$$

3. Data analysis and validation

The analysis and validation of the new model are conducted in this section, including analysis of simulation data and comparison of numerical and published experimental results. The degree of approximation between the approximate dynamic equation and system dynamic equation and the effects of m and q on the model performance are both investigated. First, a nondimensional analysis is performed to facilitate the analysis.

It should be pointed out that this paper primarily studies the contact-impact model. As one of the most important parts of the simulation of the contact-impact phenomenon, contact detection research is still a growing field but has reached some maturity, and several different methods have been developed [59,60]. The simulations in this paper are relatively simple, and the contact situations are determined by calculating the distances between the potential points and the values of indentation depth. For more complex problems, some contact detection algorithms for multibody simulations with a continuous contact force model have been proposed [59,60].

3.1. Nondimensional form of the system dynamic equation and the approximate dynamic equation

A nondimensional analysis is conducted to facilitate the comparison and analysis of the simulation results. We introduce the nondimensional variables $x = \delta/\delta_{max}$ and $\tau = t/\left(\delta_{max}/\dot{\delta}^{(-)}\right)$, and it can be deduced that [21,31]

$$\frac{d\delta}{dt} = \dot{\delta}^{(-)}\frac{dx}{d\tau} \tag{37}$$

and

$$\frac{d^2\delta}{dt^2} = \frac{(\dot{\delta}^{(-)})^2}{\delta_{max}}\frac{d^2x}{d\tau^2} \tag{38}$$

According to Eq. (37), the initial velocity of x is equal to 1.0. Substituting Eqs. (37) and (38) into the system dynamic equation shown in Eq. (1) yields

$$\frac{m_0(\dot{\delta}^{(-)})^2}{\delta_{max}}\ddot{x} + k\delta_{max}^n x^n + \lambda\delta_{max}^m x^m(\dot{\delta}^{(-)})^q\left(\frac{dx}{d\tau}\right)^q = 0 \tag{39}$$

The following nondimensional form of the system dynamic equation can be obtained:

$$\ddot{x} + k_{non}x^n + \lambda_{non}x^m(\dot{\delta}^{(-)})^q\dot{x}^q = 0 \tag{40}$$

where k_{non} and λ_{non} are the nondimensional parameters, which are described as

$$k_{non} = \frac{k\delta_{max}^{n+1}}{m_0(\dot{\delta}^{(-)})^2} \tag{41}$$

$$\lambda_{non} = \frac{\lambda\delta_{max}^{m+1}(\dot{\delta}^{(-)})^q}{m_0(\dot{\delta}^{(-)})^2} \tag{42}$$

Substituting Eq. (31) into Eqs. (41) and (42), we obtain

$$k_{non} = \frac{(n+1)({c_r}^2 + {c_r}^q)}{2(1+{c_r}^q)} \tag{43}$$

$$\lambda_{non} = \frac{\lambda(\dot{\delta}^{(-)})^q}{m_0(\dot{\delta}^{(-)})^2}\left(\frac{m_0(n+1)(\dot{\delta}^{(-)})^2}{2k}\bullet\frac{{c_r}^2+{c_r}^q}{1+{c_r}^q}\right)^{\frac{m+1}{n+1}} \tag{44}$$

Substituting Eq. (35) into Eq. (44),

$$\lambda_{non} = \frac{m_0(2+q)(1-{c_r}^2)(m+1)(\dot{\delta}^{(-)})^2}{4(\dot{\delta}^{(-)})^q(1+{c_r}^q)}\left(\frac{m_0(n+1)(\dot{\delta}^{(-)})^2}{2k}\bullet\frac{{c_r}^2+{c_r}^q}{1+{c_r}^q}\right)^{-\frac{m+1}{n+1}}\frac{(\dot{\delta}^{(-)})^q}{m_0(\dot{\delta}^{(-)})^2}\left(\frac{m_0(n+1)(\dot{\delta}^{(-)})^2}{2k}\bullet\frac{{c_r}^2+{c_r}^q}{1+{c_r}^q}\right)^{\frac{m+1}{n+1}} \tag{45}$$

Then, we obtain

$$\lambda_{non} = \frac{(m+1)(2+q)(1-{c_r}^2)}{4(1+{c_r}^q)} \tag{46}$$

Similar to the analysis for the system dynamic equation, by substituting Eqs. (35), (37) and (38) into the approximate dynamic equation shown in Eq. (36), we can obtain the nondimensional form of the approximate dynamic equation,

$$\begin{cases} \dfrac{d^2x}{d\tau^2} + (k_{non}^* + \lambda_{non}^*)x^m = 0 \text{ Compressionphase} \\ \dfrac{d^2x}{d\tau^2} + (k_{non}^* - c_r\lambda_{non}^*)x^m = 0 \text{ Restitution phase} \end{cases} \tag{47}$$

where k_{non}^* and λ_{non}^* are the nondimensional parameters, which are described as

$$k_{non}^* = \frac{(m+1)({c_r}^2+{c_r}^q)}{2(1+{c_r}^q)} \tag{48}$$

$$\lambda_{non}^* = \frac{(m+1)(2+q)(1-{c_r}^2)(\dot{\delta}^{(-)})^{1-q}}{4(1+{c_r}^q)}\left(\frac{2}{2+q}\right)^{\frac{1}{q}} \tag{49}$$

It can be determined from Eqs. (43), (46), (48) and (49) that the nondimensional parameters k_{non}, λ_{non}, k_{non}^* and λ_{non}^* depend on the exponent n, m, q, the coefficient of restitution c_r, and the initial velocity $\dot{\delta}^{(-)}$.

3.2. Simulations of the system dynamic equation and the approximate dynamic equation

To evaluate the degree of approximation between the approximate dynamic equation and system dynamic equation, a series of numerical simulations is conducted based on the nondimensional form of the approximate dynamic equation and system dynamic equation, as described in Eqs. (40) and (47).

The value of n depends on the geometric properties of contacting surfaces and is set as the most commonly used value of 1.5. As described in Section 3.1, the initial velocity of x is equal to 1.0. The values of the restitution coefficient c_r are set as 0.9, 0.6, and 0.3. The simulation is based on the fourth–order Runge–Kutta method, and the time steps are set as 1E-8 s. The respective numerical results from the nondimensional form of the system dynamic equation and approximate dynamic equation are deemed accurate and approximate.

The numerical simulations are divided into two categories. In the first type of simulation, m is set equal to n to investigate the influence of q on the approximation degree of the two equations, as shown in Fig. 4. In the second type of simulation, n is set as constant, and the influences of m and q values on the approximation degree of the two equations are examined, as shown in Fig. 5.

As shown in Fig. 4, when $m = n$ and q varies (q is set as 0.9, 1.0, and 1.1), the two equations exhibit reasonable approximations, and a higher restitution coefficient corresponds to a superior approximation degree. When the restitution coefficient is high ($c_r = 0.9$, as shown in Fig. 4(a)), the approximation degree is excellent, and the value of q has almost no effect on the approximation. As shown in Fig. 4(b), the approximation is satisfactory for the recovery factor $c_r = 0.6$, and the change in q value does not significantly influence the approximation. When the restitution coefficient is low ($c_r = 0.3$, as shown in Fig. 4(c)), the degree of approximation varies significantly, and the best degree of approximation is attained when $q = 1.0$.

As shown in Fig. 5, when m and q vary, the two equations are well approximated, and a higher recovery coefficient corresponds to a better degree of approximation. The values of m and q are set as the following five pairs: $m = 1.2$, $q = 0.9$; $m = 1.2$, $q = 1.1$; $m = 1.5$, $q = 1.0$; $m = 1.8$, $q = 0.9$; and $m = 1.8$, $q = 1.1$. When the recovery coefficient is high ($c_r = 0.9$ in Fig. 5(a)), the approximation degree is satisfactory. Compared with Fig. 4 (a), the q value exerts nearly no influence on the approximation degree of the equation, while the change in m influences the contact duration time. As shown in Fig. 5(b), when the restitution coefficient equals 0.6, the simulation

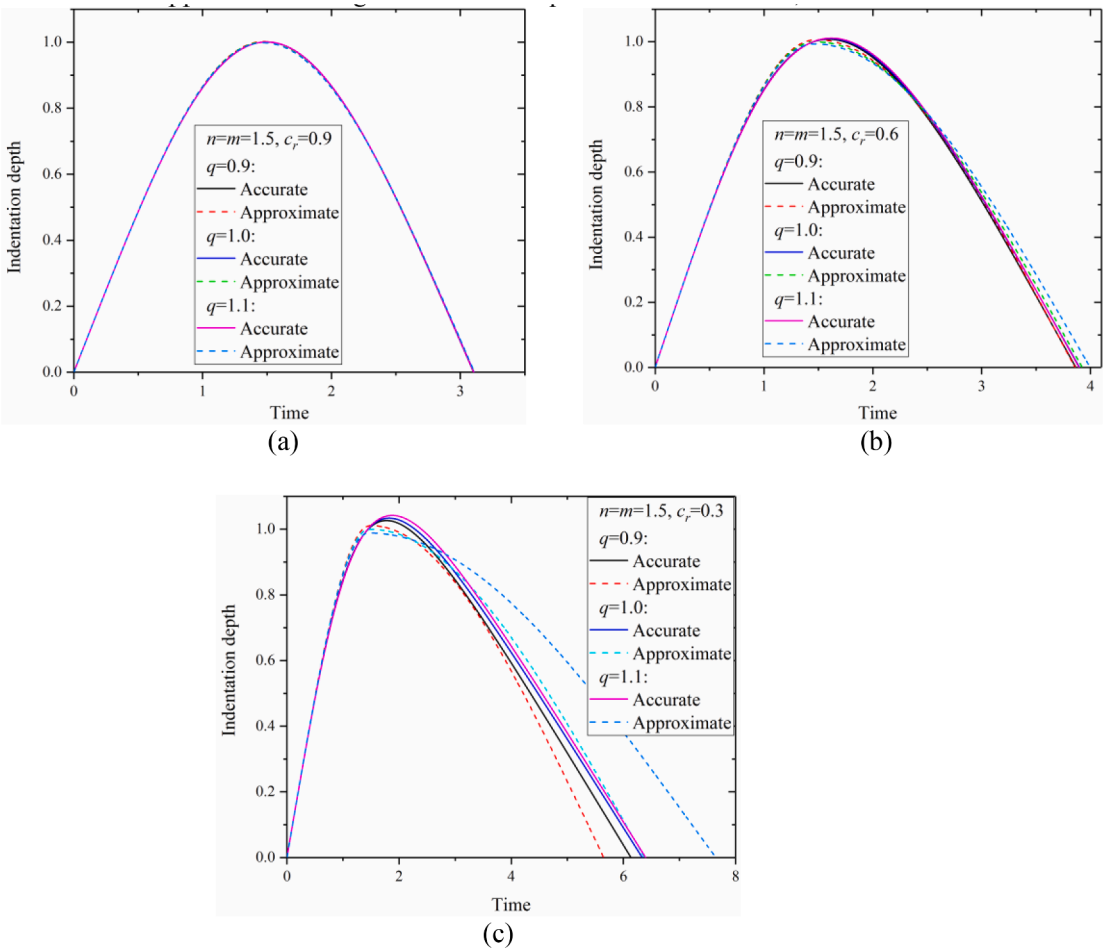

Fig. 4. Simulation results with $m = n$ and varying q: (a) $c_r = 0.9$; (b) $c_r = 0.6$; (c) $c_r = 0.3$.

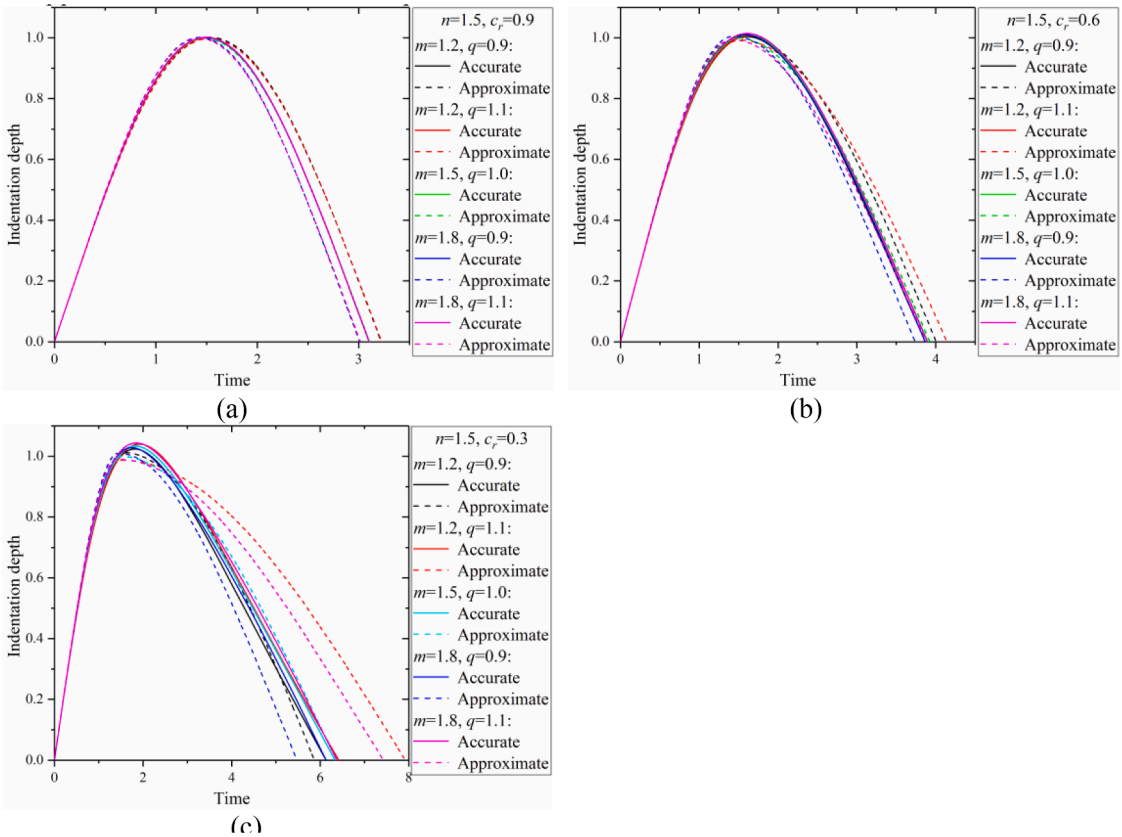

Fig. 5. Simulation results with varying m and q: (a) $c_r = 0.9$; (b) $c_r = 0.6$; (c) $c_r = 0.3$.

results obtained based on the two equations are slightly different, and the best approximation is achieved when $m = 1.5$, $q = 1.0$ and $m = 1.8$, $q = 1.1$. When the recovery coefficient is low ($c_r = 0.3$, as shown in Fig. 5(c)), the system dynamic behaviors associated with the approximate dynamic equation and system dynamic equation are different. When $m = 1.5$, $q = 1$ and $m = 1.2$, $q = 0.9$, the approximation degree is relatively high.

In conclusion, the deviation in the system dynamic behaviors associated with the approximate dynamic equation and system dynamic equation is small, and the approximate dynamic equation achieves a reasonable approximation of the system dynamic equation. Therefore, it is feasible to derive the hysteresis damping factor based on the system dynamic equation and approximate dynamic equation.

3.3. Comparisons between the simulation and experimental results

Two published experimental datasets are utilized to validate the new contact model [61,62], involving steel balls [61] and cores of leather-bound sliotar ball [62], and the influences of the m and q values on the performance of the contact models are investigated by comparing the simulation and experimental results. The collisions in both experiments are direct central normal impacts without friction, and in previous studies the relevant experiment results have been utilized to validate and compare the continuous contact models [61,62]. In this paper, three typical continuous contact models are utilized for the comparison of the model proposed in this paper, including the models developed by Hunt and Crossley [29], Lankarani and Nikravesh [36] and Jie Zhang et al. (proposed in 2020) [21]. Numerical simulations are conducted based on the system dynamic equation, as illustrated in Eq. (1). The values of n, k, c_r, m_0 and $\dot{\delta}^{(-)}$ are extracted from two published studies, and the value of the hysteresis damping factor λ is calculated according to Eq. (35). Numerical simulations are conducted based on three typical models and the new model with various m and q values. The simulation is based on the fourth-order Runge–Kutta method, and the time steps are set as 1E-8 s.

3.3.1. Impact of steel ball

An experiment involving a spherical ball impacting cylindrical specimens were conducted by Zhang and Sharf to validate the Hunt–Crossley series of models [61], in this paper it is utilized to validate the new contact model. A steel ball (mass $m_0 = 0.54$ kg) is released from a stationary position, and a direct central normal impact occurs between the ball and cylindrical specimen C2. The contact force, duration time, initial impact velocity and restitution coefficient are measured in the experiment. Details regarding the

experimental process can be found in [61]. In addition to the three previous models mentioned above, numerical simulations are conducted based on several groups of different m and q values pertaining to the classical parameters used in continuous contact models ($m = 1.5$, $q = 1.0$) and other groups of parameters ($m = 1.2$, $q = 0.9$; $m = 1.2$, $q = 1.1$; $m = 1.8$, $q = 0.9$; and $m = 1.8$, $q = 1.1$). The power exponent $n = 1.5$ and stiffness parameter $k = 2.4144\text{E}10\ \text{N/L}^{\text{n}}$ are set with reference to [61].

As shown in Table 1, when the restitution coefficient is relatively large, the simulation results obtained based on different models and exponential values are all consistent with the experimental results; as determined from Table 2, when the restitution coefficient is relatively small, the relative error in the consistency of the restitution coefficient is higher for the models proposed by Hunt and Crossley and by Lankarani and Nikravesh. As shown in Tables 1 and 2, the simulation results obtained using the new model are consistent with the experimental data, and the relative errors are less than ±5%. Notable deviation is not observed between the simulation results obtained using the classical parameters ($m = 1.5$, $q = 1.0$) and other groups of parameters ($m = 1.2$, $q = 0.9$; $m = 1.2$, $q = 1.1$; $m = 1.8$, $q = 0.9$; and $m = 1.8$, $q = 1.1$). Furthermore, compared with the duration time, the change in m and q significantly influence the maximum contact force. When $m = 1.2$ and $q = 1.1$, the smallest deviation is observed between the numerical and experimental results of the maximum contact force.

The model proposed by Jie Zhang et al. in 2020 can be considered a special case of the model proposed in this paper (m and q are taken as 1.5 and 1.0, respectively), with the primary difference being that the model proposed by Jie Zhang in 2020 includes a minor adjustment to the equivalent velocity, resulting in very high accuracy in terms of consistency of restitution coefficients, as shown in Tables 1 and 2. It should be noted that when m and q are set for the model proposed in this paper, a more accurate model can be constructed by slightly adjusting the equivalent velocity based on the consistency of the restitution coefficients before and after the simulation, and thus can provide a good simulation of the velocity changes before and after a collision and the system kinematics. Additional details regarding this aspect can be found in the relevant articles [21,31]. Because both m and q are variable within a wide range of values within this paper, the optimization of the new model is not conducted in this paper.

3.3.2. *Impact of the cores of leather-bound sliotar ball*

Relative to the steel ball impact experiment, an impact experiment with more complex materials, faster impact velocities and lower restitution coefficients is used to validate the new model and investigate the effects of m and q values on the model accuracy, this experiment was previously conducted to investigate the Hunt and Crossley model and modified Kelvin-Voigt model [62]. The collision in the experiment occurs between sliotar cores and fixed rigid steel impact plate. The sliotar, a small leather-bound ball consisting of leather skin and a solid core, is used in the Irish sport of hurling. Four sliotar cores (labeled A, B, C and D) with different materials were selected in [62]. Table 3 quantifies the dimensions, masses, compositions and k and c_r values of these cores. The power exponent $n = 1.5$, and the initial impact velocity is 15 m/s. More details regarding the experiment can be found in [62]. A series of numerical simulations is conducted based on the three previous models mentioned above and various m and q values of the new model of this paper. As shown in Table 3, the parameters in the numerical simulations are set with reference to [62]. The comparison between the simulation and experimental results shows that the optimal parameters are $m = 1.1$ and $q = 1.25$. Fig. 6 shows plots of the indentation depth vs. contact force for each ball type, as recorded experimentally and predicted by the models. Except for the three previous models, numerical simulations are conducted based on the new model with two sets of parameters: the classical parameters used in continuous contact models ($m = 1.5$, $q = 1.0$) and optimal parameters in this numerical example ($m = 1.1$, $q = 1.25$). A detailed analysis is conducted to evaluate the influences of the m and q values on the performance of the continuous contact force models.

The comparison between the simulation and experimental results shows that the performance of the continuous contact model can be improved by selecting appropriate values of m and q. As illustrated in Fig. 6, the simulation results obtained based on the Hunt and Crossley model and the Lankarani and Nikravesh model significantly deviate from the experimental values. As for the maximum contact force, the relative errors of balls A, B, C and D are about 15.5%, 10.5%, 10.3% and 7.8%, respectively, and for the maximum indentation depth, the relative errors are about 17.5%, 13.3%, 14.0% and 11.4%, respectively.

Fig. 6 also shows that the simulation results obtained based on the new model with classical parameters ($m = 1.5$, $q = 1.0$) and the model proposed by Jie Zhang in 2020 deviate from the experimental values in the simulation of the maximum contact force, and the relative errors of the maximum contact forces of balls A, B, C and D are about 17.9%, 12.5%, 12.3% and 9.5%, respectively. In contrast,

Table 1
Comparison of the numerical and experimental results with initial impact velocity 0.15 m/s.

	c_r	Relative error [%]	Duration time (10E-4 *s*)	Relative error [%]	Maximum contact force (*N*)	Relative error [%]
Experiment results [61]	0.8892		2.52		1076.6	
The model in this paper:						
$m = 1.5$, $q = 1.0$	0.8891	−0.02	2.620	3.97	1089.8	1.23
$m = 1.2$, $q = 0.9$	0.8886	−0.07	2.618	3.89	1088.9	1.15
$m = 1.2$, $q = 1.1$	0.8880	−0.13	2.618	3.89	1080.6	0.37
$m = 1.8$, $q = 0.9$	0.8945	0.60	2.618	3.89	1100.9	2.26
$m = 1.8$, $q = 1.1$	0.8950	0.66	2.616	3.81	1090.6	1.30
Hunt and Crossley [29]	0.9002	1.23	2.614	3.71	1095.0	1.71
Lankarani and Nikravesh [36]	0.9052	1.80	2.612	3.65	1097.4	1.93
Jie Zhang et al. (2020) [21]	0.8892	−0.00	2.618	3.87	1089.9	1.23

Table 2
Comparison of the numerical and experimental results with initial impact velocity 0.5 m/s.

	c_r	Relative error [%]	Duration time (10E-4 s)	Relative error [%]	Maximum contact force (N)	Relative error [%]
Experiment results [61]	0.7568		2.07		4364.6	
The model in this paper:						
$m = 1.5$, $q = 1.0$	0.7553	−0.19	2.106	1.74	4447.0	1.89
$m = 1.2$, $q = 0.9$	0.7548	−0.26	2.104	1.64	4419.2	1.25
$m = 1.2$, $q = 1.1$	0.7540	−0.38	2.102	1.55	4322.2	−0.97
$m = 1.8$, $q = 0.9$	0.7665	1.29	2.102	1.55	4581.7	4.97
$m = 1.8$, $q = 1.1$	0.7673	1.39	2.098	1.35	4474.2	2.51
Hunt and Crossley [29]	0.8036	6.19	2.085	0.72	4491.3	2.90
Lankarani and Nikravesh [36]	0.8234	8.80	2.078	0.38	4515.5	3.46
Jie Zhang et al. (2020) [21]	0.7564	−0.05	2.103	1.60	4447.7	1.90

Table 3
The basic parameters of the experiment [62].

Ball ID	Diameter (mm)	Mass m_0 (g)	Material mass composition	Contact stiffness k (N/m$^{1.5}$ × 10^6)	Restitution coefficient c_r
A	66.2 ± 0.1	89.6 ± 0.4	100% polyurethane-based polymer	3.50	0.527
B	66.8 ± 0.2	89.9 ± 3.1	100% polyurethane-based polymer	2.85	0.535
C	65.6 ± 0.1	89.1 ± 0.9	Cork (81%), yarn (19%)	5.65	0.533
D	68.2 ± 0.4	83.1 ± 0.3	Cork (38%), polyester (38%), yarn (24%)	3.70	0.546

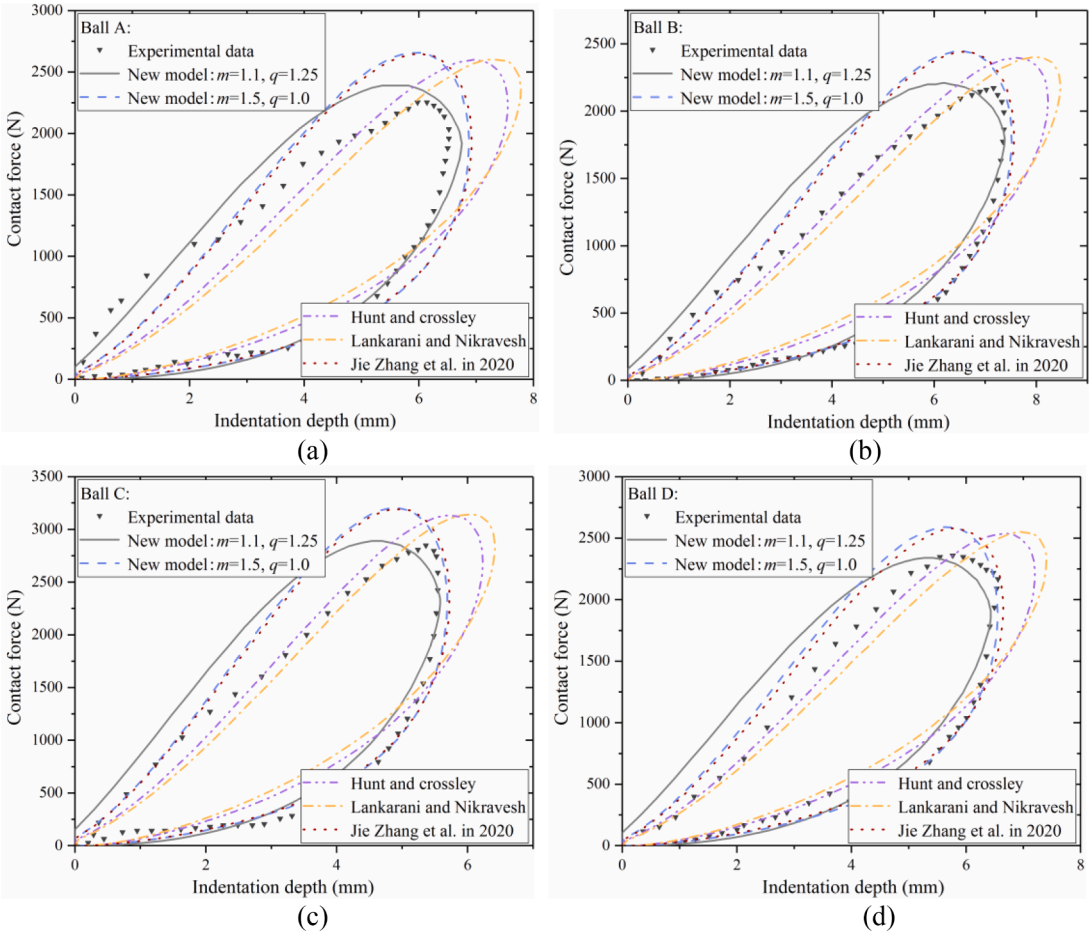

Fig. 6. Comparison between the numerical and experimental results for the impacts of four leather-bound sliotar balls.

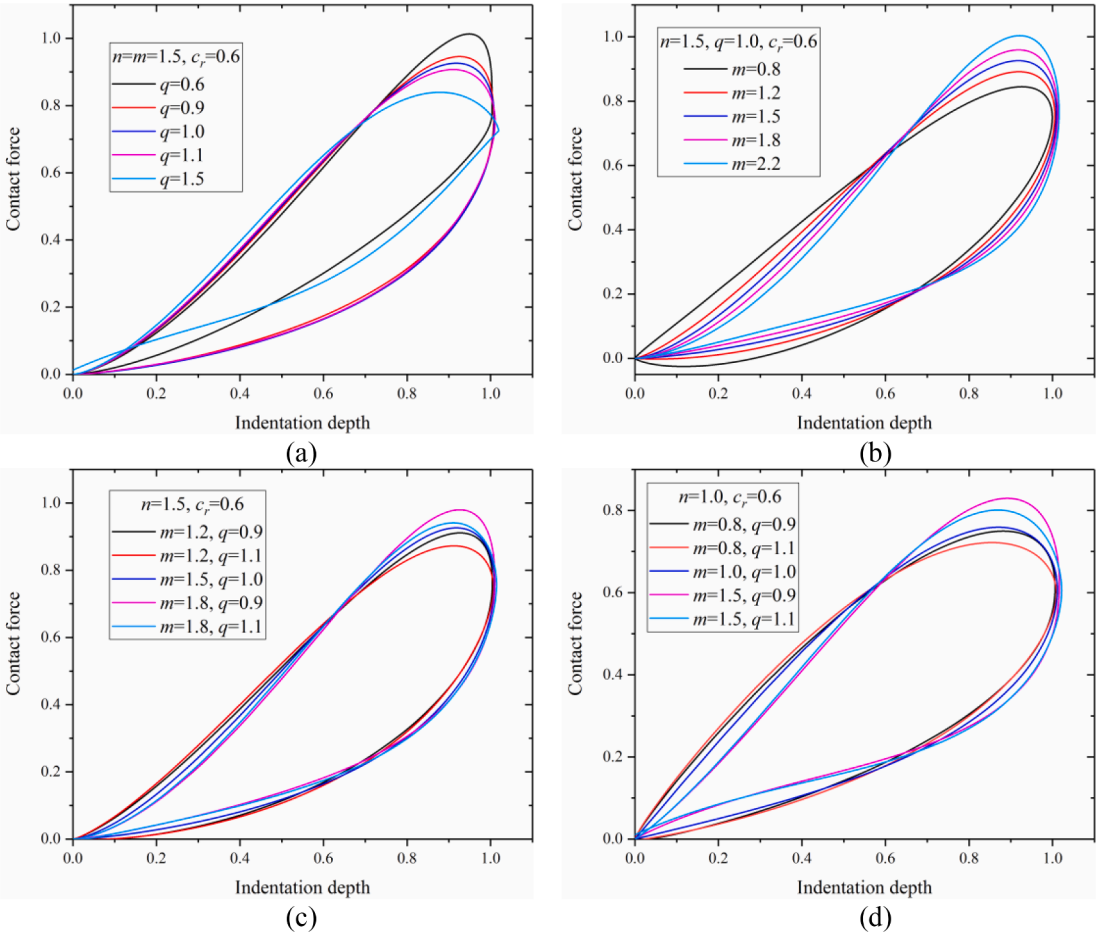

Fig. 7. Simulation results with different parameters (a) $m = n = 1.5$, $c_r = 0.6$, q varies; (b) $n = 1.5$, $q = 1.0$, $c_r = 0.6$, m varies; (c) $n = 1.5$, $c_r = 0.6$, m and q vary; (d) $n = 1.0$, $c_r = 0.6$, m and q vary; (e) $n = 2.0$, $c_r = 0.6$, m and q vary; (f) $n = 1.5$, $c_r = 0.9$, m and q vary; (g) $n = 1.5$, $c_r = 0.3$, m and q vary.

the simulations of the maximum indentation depth were relatively accurate, with relative errors of about 5.7%, 2.4%, 2.9%, and 0.7%, respectively.

When the optimal parameters ($m = 1.1$, $q = 1.25$) are used for the new model, a certain deviation remains between the simulation and experimental results; however, the relative errors of the maximum contact force are reduced to 6.3%, 1.6%, 1.4% and −0.9%, respectively. And the relative errors of the maximum indentation depths are about 3.4%, 0.2%, 0.7% and −1.9%, respectively.

Therefore, by selecting appropriate values of m and q, the performance of the continuous contact model can be improved, and the simulation results can approach the experimental results. Notably, a certain deviation remains between the experimental results and the shape of the indentation depth vs. contact force curve obtained in the simulation based on the optimal parameters. The series of simulations shows that it is difficult to find a set of parameters for which the simulation results match the experimental results in all aspects. This shows the limitation of the contact force model constructed based on the general contact force expression.

The comparison between the simulation and two sets of published experimental results demonstrates the validity and potential of the new model. In the case of the impact of steel balls, the simulation results obtained using the new model are consistent with the experimental data, and the relative errors of the simulation results obtained based on different m and q values are less than ±5%. The comparison between the simulation and experimental results for the case of the cores of leather-bound sliotar ball shows that the new model proposed in this paper has better simulation accuracy than the previous models, it also reveals that the performance of the continuous contact model can be improved by selecting appropriate values of m and q.

3.4. Influences of the values of exponents on the contact models

To evaluate the influences of the m and q values on the performance of the continuous contact force models, a series of numerical simulations is conducted based on the nondimensional form of the system dynamic equation, as described in Eq. (40).

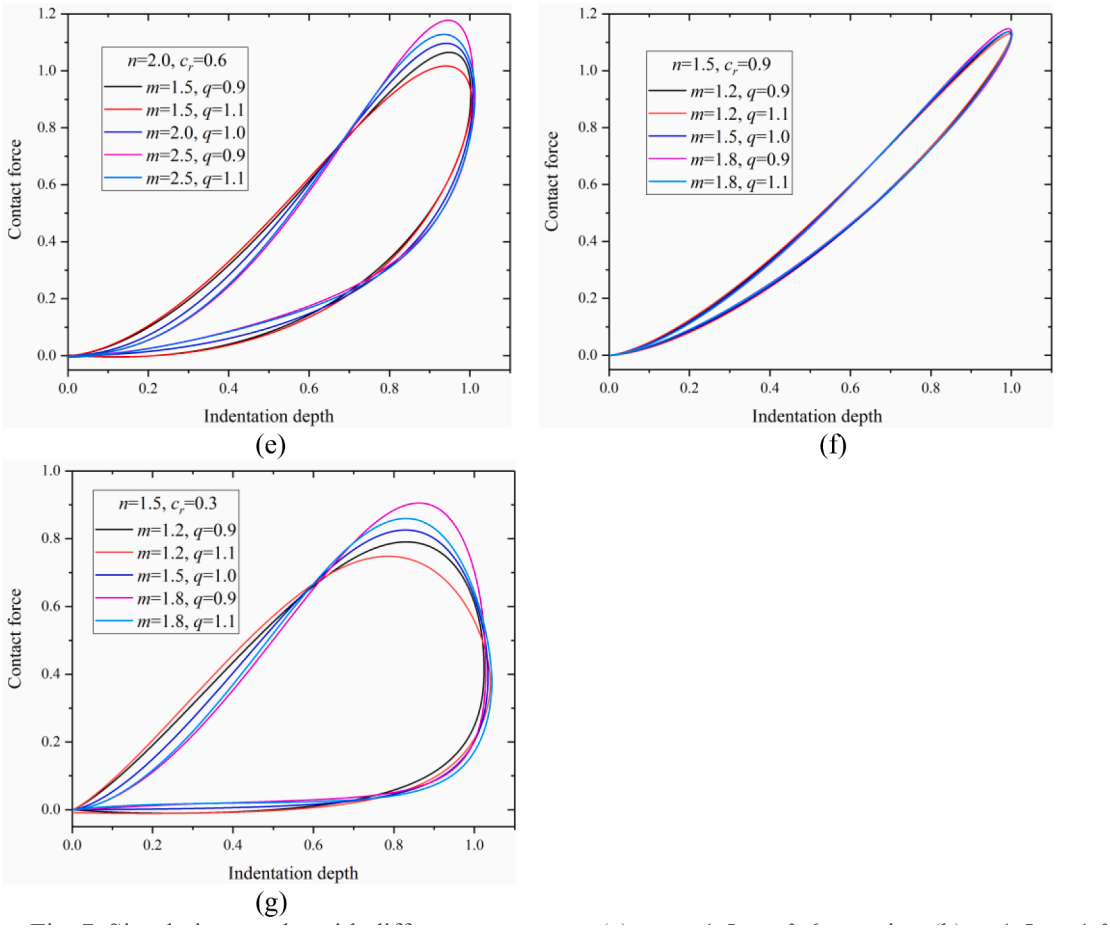

Fig. 7. (*continued*).

The simulation is based on the fourth-order Runge–Kutta method, and the time steps are set as 1E-8 *s*. According to the analysis in Section 3.1, the initial velocity of x is equal to 1.0. Based on the simulation results of five sets of parameters, plots of the indentation depth vs. contact force are obtained, and detailed analyses are conducted. The corresponding specific parameter values and simulation results are shown in Fig. 7.

In the first set of parameters, the values of m, n and c_r are set to study the influence of q on the performance of the contact model, as shown in Fig. 7(a) ($m = n = 1.5$, $c_r = 0.6$ and $q = 0.6$, 0.9, 1.0, 1.1 or 1.5). A smaller q corresponds to a larger maximum contact force obtained in the simulation. The influence of q on the maximum indentation depth is almost negligible. In addition, the variation in q value exerts a certain effect on *the* shape of the indentation depth–contact force curve.

In the second set of parameters, the values of n, q and c_r are set to study the influence of m on the performance of the contact model, as shown in Fig. 7(b) ($n = 1.5$, $q = 1.0$, $c_r = 0.6$ and $m = 0.8$, 1.2, 1.5, 1.8 or 2.2). A smaller m value corresponds to a larger maximum contact force obtained in the simulation. The influence of m on the maximum indentation depth is almost negligible. In addition, the variation in the m value exerts a certain effect on the shape of the indentation depth–contact force curve.

In the third set of parameters, the values of n and c_r are set to study the influence of m and q on the performance of the contact model, as shown in Fig. 7(c) ($n = 1.5$, $c_r = 0.6$, and the values of m and q are set in five pairs: $m = 1.2$, $q = 0.9$; $m = 1.2$, $q = 1.1$; $m = 1.5$, $q = 1.0$; $m = 1.8$, $q = 0.9$; and $m = 1.8$, $q = 1.1$). Larger m and smaller q correspond to a larger maximum contact force. The influences of m and q on the maximum indentation depth are almost negligible. In addition, the variations in m and q have a certain effect on the shape of the indentation depth–contact force curve.

In the fourth set of parameters, for different values of n, the value of c_r is set to study the influence of m and q on the performance of the contact model, as shown in Fig. 7(d) ($n = 1.0$, $c_r = 0.6$, the values of m and q are set in five pairs: $m = 0.8$, $q = 0.9$; $m = 0.8$, $q = 1.1$; $m = 1.0$, $q = 1.0$; $m = 1.5$, $q = 0.9$; and $m = 1.5$, $q = 1.1$) and Fig. 7(e) ($n = 2.0$, $c_r = 0.6$, and the values of m and q are set in five pairs: $m = 1.5$, $q = 0.9$; $m = 1.5$, $q = 1.1$; $m = 2.0$, $q = 1.0$; $m = 2.5$, $q = 0.9$; and $m = 2.5$, $q = 1.1$). A larger n corresponds to a larger maximum contact force. The effect of m and q on the model performance is similar to that in the third set of parameters. Moreover, the variation in n exerts a certain effect on the shape of the indentation depth–contact force curve.

In the fifth set of parameters, for different values of c_r, the value of n is set to study the influence of m and q on the performance of

the contact model, as shown in Fig. 7(f-g) ($n = 1.5$, $c_r = 0.9$ or 0.3, and the values of m and q are set in five pairs: $m = 1.2$, $q = 0.9$; $m = 1.2$, $q = 1.1$; $m = 1.5$, $q = 1.0$; $m = 1.8$, $q = 0.9$; and $m = 1.8$, $q = 1.1$). According to Fig. 7(f-g), a smaller restitution coefficient exerts more significant effects of m and q on the contact model performance. Moreover, a larger m and smaller q correspond to a larger maximum contact force. The influences of m and q on the maximum indentation depth are almost negligible.

Overall, the values of m and q influence the maximum contact force obtained in the simulation, while the effect on the indentation depth is almost negligible. A larger m and smaller q correspond to a larger maximum contact force. In addition, the variation in m and q influences the shape of the indentation depth–contact force diagram. A smaller restitution coefficient corresponds to more significant effects of m and q on the contact model performance.

4. Conclusions

A general expression of the contact force, $F_c = k\delta^n + \lambda\delta^m\dot{\delta}^q$, was proposed by Hunt and Crossley in 1975. Because this expression cannot be used to find an analytical solution, more than twenty continuous contact force models have been developed based on the simplification of the general expression of the contact force. In these studies, the parameter q is set as 1.0. It is of significance to develop a contact model based on the general expression with arbitrary values of parameters m and q.

Based on the rule of energy equivalence, an approximate dynamic equation is developed, and a new continuous contact force model with arbitrary exponents n, m and q is constructed based on the general expression of the contact force. The new model is validated by comparing the simulation results and two published experimental datasets. The analysis of simulation results shows that m and q exert nonnegligible influences on the performance of the continuous contact force models. Larger m and smaller q correspond to a larger maximum contact force. Moreover, with a smaller restitution coefficient, the effects of m and q on the contact model performance are more significant. The comparison between the simulation and experimental results indicates that the performance of the continuous contact model can be improved by selecting appropriate values of m and q.

CRediT authorship contribution statement

Jie Zhang: Methodology, Writing. **Xu Liang:** Data curation. **Zhonghai Zhang:** Data curation. **Guanhua Feng:** Formal analysis, Writing – review & editing. **Quanliang Zhao:** Writing – review & editing. **Lei Zhao:** Visualization. **Guangping He:** Supervision, Writing – review & editing.

Declaration of Competing Interest

The authors declare that they have no known competing financial interests or personal relationships that could have appeared to influence the work reported in this paper.

Acknowledgements

This research was supported by the National Key R&D Program of China [grant number 2019YFB1309603]; the National Natural Science Foundation of China [grant numbers 11702294, 62103007]; the Guangdong Province key research and development project [grant number 2021B0101240001]; the Joint Program of Beijing Municipal Foundation and Education Commission [grant number KZ202010009015]; the Frontier Scientific and Technological Innovation Funded Project of National Key R&D Program of China [grant number 2019QY(Y)0402]; the Beijing Natural Science Foundation [grant number L202020]; and the Scientific Research Foundation of North China University of Technology. The author would like to thank American Journal Experts for their English corrections.

References

[1] G. Gilardi, I. Sharf, Literature survey of contact dynamics modelling, Mech. Mach. Theory 37 (10) (2002) 1213–1239, https://doi.org/10.1016/s0094-114x(02)00045-9.
[2] E. Corral, R.G. Moreno, M.J.G. García, et al., Nonlinear phenomena of contact in multibody systems dynamics: a review, Nonlinear Dyn. 104 (2) (2021) 1269–1295, https://doi.org/10.1007/s11071-021-06344-z.
[3] Z. Zhao, C.S. Liu, N.N. Wang, Rocking dynamics of a planar rectangular block on a rigid surface, Multibody Syst. Dyn. 45 (2019) 105–125, https://doi.org/10.1007/s11044- 018-09643-3.
[4] J. Ma, S. Dong, G. Chen, et al., A data-driven normal contact force model based on artificial neural network for complex contacting surfaces, Mech. Syst. Signal PR. 156 (3) (2021), https://doi.org/10.1016/j.ymssp.2021.107612.
[5] X. Zheng, F. Zhang, Q. Wang, Modeling and simulation of planar multibody systems with revolute clearance joints considering stiction based on an LCP method, Mech. Mach. Theory 130 (2018) 184–202, https://doi.org/10.1016/j.mechmachtheory.2018.08.017.
[6] Z. Zhao, C.S. Liu, T. Chen, Docking dynamics between two spacecrafts with APDSes, Multibody Syst. Dyn. 37 (3) (2016) 245–270, https://doi.org/10.1007/s11044-015-9477-4.
[7] R. Zhang, Y. Yu, Q. Wang, et al., An improved implicit method for mechanical systems with set-valued friction, Multibody Syst. Dyn. (2019) 1–28, https://doi.org/10.1007/s11044-019-09713- 0.
[8] X.F. Liu, G.P. Cai, M.M. Wang, et al., Contact control for grasping a non-cooperative satellite by a space robot, Multibody Syst. Dyn. 50 (2) (2020) 119–141, https://doi.org/10.1007/s11044-020-09730-4.
[9] Z. Zhou, X.D. Zheng, Q. Wang, Modeling and simulation of point contact multibody system dynamics based on the 2D LuGre friction model, Mech. Mach. Theory 158 (2021), 104244, https://doi.org/10.1016/j.mechmachtheory. 2021.104244.
[10] S. Luka, S. Janko, B. Miha, A review of continuous contact-force models in multibody dynamics, Int. J. Mech. Sci. 145 (2018) 171–187, https://doi.org/10.1016/j.ijmecsci.2018.07.010.

[11] A. Banerjee, A. Chanda, R. Das, Historical origin and recent development on normal directional impact models for rigid body contact simulation: a critical review, Arch. Comput. Method E. 24 (2) (2017) 397–422, https://doi.org/10.1007/s11831-016-9164-5.
[12] C.S. Koshy, P. Flores, H.M. Lankarani, Study of the effect of contact force model on the dynamic response of mechanical systems with dry clearance joints: computational and experimental approaches, Nonlinear Dyn. 73 (1–2) (2013) 325–338, https://doi.org/10.1007/s11071-013-0787-x.
[13] M. Molotskii, I. Torchinsky, G. Rosenman, Hertz model for contact of water droplet with superhydrophobic surface, Phys. Lett. A 373 (8–9) (2009) 804–806, https://doi.org/10.1016/j.physleta.2009.01.001.
[14] X.F. Liu, X.Y. Zhang, G.P. Cai, et al., A collision control strategy for detumbling a non-cooperative spacecraft by a robotic arm, Multibody Syst. Dyn. (2021) 1–31, https://doi.org/10.1007/s11044-021-09793-x.
[15] S. Ken, Newton's cradle versus nonbinary collisions, Phys. Rev. Lett. 104 (12) (2010), https://doi.org/10.1103/physrevlett.104.124302.
[16] J. Horabik, M. Beczek, R. Mazur, et al., Determination of the restitution coefficient of seeds and coefficients of visco-elastic Hertz contact models for DEM simulations, Biosyst. Eng. 161 (2017) 106–119, https://doi.org/10.1016/j.biosystemseng.2017.06.009.
[17] J. Sun, N. Lam, L. Zhang, et al., A note on Hunt and Crossley model with generalized visco-elastic damping, Int. J. Impact Eng. 121 (2018) 151–156, https://doi.org/10.1016/j.ijimpeng.2018.07.007.
[18] D. Cao, Y. Yang, H. Chen, et al., A novel contact force model for the impact analysis of structures with coating and its experimental verification, Mech. Syst. Signal PR 70–71 (2016) 1056–1072, https://doi.org/10.1016/j.ymssp. 2015.08.016.
[19] J. Ma, G. Chen, L. Ji, et al., A general methodology to establish the contact force model for complex contacting surfaces, Mech. Syst. Signal PR. 140 (2020), 106678, https://doi.org/10.1016/j.ymssp.2020.106678.
[20] H. Hertz, Ueber die beruehrung fester elastischer koerper, J. Reine Angew. Math. 91 (1881) 156–171, https://doi.org/10.1515/crll.1882.92.156.
[21] J. Zhang, W. Li, L. Zhao, et al., A continuous contact force model for impact analysis in multibody dynamics, Mech. Mach. Theory 153 (2020), 103946, https://doi.org/10.1016/j. mechmachtheory.2020.103946.
[22] K.L. Johnson, One hundred years of Hertz contact, Proc. Inst. Mech. Eng. 196 (1982) 363–378, https://doi.org/10.1243/pime_proc_1982_196_039_02.
[23] V.L. Popov, Contact Mechanics and Friction, first ed., Springer Berlin Heidelberg, Berlin, 2010.
[24] W. Thompson, On the elasticity and viscosity of metals, Proc. Roy. Soc. London 14 (1865) 289–297, https://doi.org/10.1098/rspl.1865.0052.
[25] W. Voigt, Ueber die specifische wärme fester körper, insbesondere der metalle, Springer Berlin Heidelberg, Berlin, 1892.
[26] P. Flores, M. Machado, M.T. Silva, et al., On the continuous contact force models for soft materials in multibody dynamics, Multibody Syst. Dyn. 25 (3) (2011) 357–375, https://doi.org/10.1007/s11044-010-9237-4.
[27] B. Brogliato, Nonsmooth Mechanics. Models, Dynamics and Control, third ed., Springer, Switzerland, 2016.
[28] R. Simon, The development of a mathematical tool for evaluating golf club performance, in: Proceedings of ASME Design Engineering Conference, New York city, USA (1967).
[29] K.H. Hunt, F.R.E. Crossley, Coefficient of restitution interpreted as damping in vibroimpact, J. Appl. Mech. 42 (2) (1975) 440–445, https://doi.org/10.1115/1.3423596.
[30] M.R. Silva, F. Marques, M.T. Silva, et al., A compendium of contact force models inspired by Hunt and Crossley's cornerstone work, Mech. Mach. Theory 167 (2022), 104501, https://doi.org/10.1016/j.mechmachtheory.2021.104501.
[31] J. Zhang, H. Can, L. Zhao, et al., Continuous contact force model with an arbitrary damping term exponent: model and discussion, Mech. Syst. Signal PR. 159 (2021), https://doi.org/10.1016/j.ymssp.2021.107808.
[32] H. Safaeifar, A. Farshidianfar, A new model of the contact force for the collision between two solid bodies, Multibody Syst. Dyn. 50 (2020) 233–257, https://doi.org/10.1007/s11044-020-09732-2.
[33] S. Hu, X. Guo, A dissipative contact force model for impact analysis in multibody dynamics, Multibody Syst. Dyn. 35 (2) (2015) 131–151, https://doi.org/10.1007/s11044-015-9453-z.
[34] Y. Shen, D. Xiang, X. Wang, et al., A contact force model considering constant external forces for impact analysis in multibody dynamics, Multibody Syst. Dyn. 44 (4) (2018) 397–419, https://doi.org/10.1007/s11044-018-09638-0.
[35] R.G. Herbert, D.C. McWhannell, Shape and frequency composition of pulses from an impact pair, J. Eng. Ind. 99 (1977) 513-518. https://doi. org/10.1115/1.3439270.
[36] H.M. Lankarani, P.E. Nikravesh, A contact force model with hysteresis damping for impact analysis of multibody systems, J. Mech. Des. 112 (3) (1990) 369–376, https://doi.org/10.1115/1. 2912617.
[37] Y. Gonthier, J. McPhee, C. Lange, et al., A regularized contact model with asymmetric damping and dwell-time dependent friction, Multibody Syst. Dyn. 11 (3) (2004) 209–233, https://doi.org/10.1023/B:MUBO.0000029392.21648.bc.
[38] Y. Zhang, I. Sharf, Compliant force modeling for impact analysis, Proceedings of the 2004 ASME International Design Technical Conference, Salt Lake City, UT. https://doi.org/10.1115/DETC2004-57220.
[39] D.W. Marhefka, D.E. Orin, A compliant contact model with nonlinear damping for simulation of robotic systems, IEEE Trans. Syst. Man Cybern. Syst. Hum. 29 (1999) 566–572, https://doi.org/10.1109/3468.798060.
[40] Q. Zhiying, L. Qishao, Analysis of impact process based on restitution coefficient, J. Dyn. Control 4 (2006) 294–298.
[41] M. Bordbar, T. Hyppänen, Modeling of binary collision between multisize viscoelastic spheres, J. Numer. Anal. Ind. Appl. Math. 2 (3–4) (2007) 115–128.
[42] J. Yu, J. Chu, Y. Li, et al. An improved compliant contact force model using a piecewise function for impact analysis in multibody dynamics, P. I. Mech. Eng. K-J. Mul. 234 (2) (2020). https://doi.org/10.1177/1464419319900874.
[43] G.X. Wang, C.S. Liu, Further investigation on improved viscoelastic contact force model extended based on hertz's law in multibody system, Mech. Mach. Theory 153 (2020), https://doi.org/10.1016/j.mechmachtheory.2020.103986.
[44] A.M. Poursina, P.E. Nikravesh, Characterization of the optimal damping coefficient in the continuous contact model, J. Comput. Nonlin. Dyn. 15 (9) 2020. https://doi.org/10.1115/1.4047136.
[45] P.Y. Zhao, J.G. Liu, Y.M. Li, et al., A spring-damping contact force model considering normal friction for impact analysis, Nonlinear Dyn. 105 (2021) 1437–1457, https://doi.org/10.1007/s11071-021-06660-4.
[46] A.S. Carvalho, J.M. Martins, Exact restitution and generalizations for the Hunt-Crossley contact model, Mech. Mach. Theory 139 (2019) 174–194, https://doi.org/10.1016/j.mechmachtheory.2019.03.028.
[47] Y. Tsuji, T. Tanaka, T. Ishida, Lagrangian numerical simulation of plug flow of cohesionless particles in a horizontal pipe, Powder Technol. 71 (3) (1992) 239–250, https://doi.org/10.1016/0032-5910(92)88030-L.
[48] G. Kuwabara, K. Kono, Restitution coefficient in a collision between two spheres, Jpn. J. Appl. Phys. 26 (8R) (1987) 1230, https://doi.org/10.1143/JJAP.26.1230.
[49] N.V. Brilliantov, F. Spahn, J.M. Hertzsch, et al., Model for collisions in granular gases, Phys. Rev. E 53 (5) (1996) 5382–5392, https://doi.org/10.1103/physreve.53.5382.
[50] N.V. Brilliantov, F. Spahn, J.M. Hertzsch, et al., The collision of particles in granular systems, Phys. A 231 (4) (1996) 417–424, https://doi.org/10.1016/0378-4371(96)00099-4.
[51] T. Schwager, T. Poschel, Coefficient of normal restitution of viscous particles and cooling rate of granular gases, Phys. Rev. E 57 (1) (1998) 650–654, https://doi.org/10.1103/PhysRevE.57.650.
[52] J. Lee, H.J. Herrmann, Angle of repose and angle of marginal stability: molecular dynamics of granular particles, J. Phys. A: Math. Gen. 26 (2) (1993) 373, https://doi.org/10.1088/0305-4470/26/ 2/021.
[53] G.H. Ristow, Simulating granular flow with molecular dynamics, J. Phys. I Fr. 2 (1992) 649–662, https://doi.org/10.1051/jp1:1992159.
[54] R. Jankowski, Analytical expression between the impact damping ratio and the coefficient of restitution in the non-linear viscoelastic model of structural pounding, Earthq. Eng. Struct. Dyn. 35 (4) (2006) 517-524. https://doi.org/10.1002/eqe.537.

[55] S. Sundar, J.T. Dreyer, R. Singh, Estimation of impact damping parameters for a cam–follower system based on measurements and analytical model, Mech. Syst. Signal PR. 81 (2016) 294–307, https://doi.org/10.1016/j.ymssp.2016.02.033.
[56] E. Alizadeh, F. Bertrand, J. Chaouki, Development of a granular normal contact force model based on a non-Newtonian liquid filled dashpot, Powder Technol. 237 (2013) 202–212, https://doi.org/10.1016/j.powtec.2013.01. 027.
[57] L. Ding, H.B. Gao, Z.Q. Deng, et al., Foot-terrain interaction mechanics for legged robots: modeling and experimental validation, J. Comput. Nonlin. Dyn. 32 (13) (2013) 1585–1606, https://doi.org/10.1177/0278364913498122.
[58] H.M. Lankarani, P.E. Nikravesh, Continuous contact force models for impact analysis in multibody systems, Nonlinear Dyn. 5 (1994) 193–207, https://doi.org/10.1007/BF00045676.
[59] P. Flores, J. Ambrósio, On the contact detection for contact-impact analysis in multibody systems, Multibody Syst. Dyn. 24 (2010) 255–280, https://doi.org/10.1007/s11044-010-9209-8.
[60] J. Choi, H.S. Ryu, C.W. Kim, et al., An efficient and robust contact algorithm for a compliant contact force model between bodies of complex geometry, Multibody Syst. Dyn. 23 (2010) 99–120, https://doi.org/10.1007/s11044-009-9173-3.
[61] Y. Zhang, I. Sharf, Validation of nonlinear viscoelastic contact force models for low speed impact, J. Appl. Mech.-T. Asme. 76 (5) (2009), https://doi.org/10.1115/1.3112739.
[62] K. Hanley, F. Collins, K. Cronin, et al., Simulation of the impact response of a sliotar core with linear and non-linear contact models, Int. J. Impact Eng. 50 (50) (2012) 113–122, https://doi.org/10.1016/j.ijimpeng.2012.06.006.